Practical Limits on the Maximal Speed of Solution Exchange for Patch Clamp Experiments

Frederick Sachs
Department of Physiology and Biophysics, State University of New York at Buffalo, Buffalo, New York 14214 USA

ABSTRACT Studying ligand-gated ion channels often requires the ability to change solutions quickly. Using finite element models, I have examined the practical limitations of how fast solutions can be exchanged on an outside-out patch using a dual stream switcher. The primary factors controlling the speed of response are the flow velocity, proximity of the patch to the exit ports, the width of the partition between the two streams, the velocity with which the streams can be moved across the patch, and the viscosity of the solutions. The practical limit seems to be a rise time of ~20 μs. The rate-limiting step is the velocity of the (usually piezo) motor that translates the streams across the patch. Increasing the perfusate viscosity improves speed by slowing dissipation of the concentration gradients. A flow switcher can also be used for bipolar temperature jumps with a rise time of ~100 μs.

INTRODUCTION

The patch clamp has provided a magnificent tool to study ion channels and ligand-receptor interactions permitting one to study channel kinetics with time resolutions approaching 10 μs (Benndorf, 1995). The ability to change reaction conditions more rapidly than the intrinsic relaxation time of the channels is essential to understanding the kinetic structure of the reaction scheme. Because molecular rate constants are functions of free energy, changing this energy in a steplike manner allows similar changes to the rates, and this allows the system to evolve in an unperturbed manner. To be generally useful, the perturbations must be rapid compared to the relaxation time of the system. If the rates are driven too slowly, the rate constants will be changing in time, and analysis requires a deconvolution of the response and the stimulus. Slow stimuli may not have sufficient power at high frequencies to resolve the faster components.

Single channel studies done at a constant mean value of the stimulus use thermally driven perturbations to excite the relevant kinetics. While this method has the least possible perturbations, slow inactivation processes may populate unresponsive states. Furthermore, stationary kinetic analysis is insensitive to the kinetics of aggregated states distant from states with different conductance (Horn and Vandenberg, 1984). By varying the stimulus intensity the rates can be driven, thereby increasing the kinetic resolution (Kienker, 1989).

For ligand gated ion channels, or channels whose gating is modified by diffusible ligands, nonstationary experiments require rapid changes in ligand concentration. These experiments are typically carried out on voltage-clamped cells or excised patches. Excised patches are smaller than cells and hence the diffusion-limited steps are faster. Inside-out patches have an intrinsic diffusional delay caused by the patch being located as many as tens of micrometers up from the tip (Sokabe et al., 1991). Outside-out patches are smaller (Sakmann and Neher, 1984; Ruknudin et al., 1991) and the active surface is exposed to the bath, so they are the membrane preparation most amenable to rapid perturbations. The ability to change solutions quickly has been used, for example, to study the population of partially liganded states of ion channels (Jonas, 1995; Maconochie et al., 1994; Colquhoun et al., 1992). Concentration jumps from low to high concentration emphasize the binding and activation steps, whereas jumps from high to low concentration emphasize the deactivation and dissociation steps. Kinetic studies can be performed on patches with many channels where the mean currents and variance analysis provide the relevant parameters. These studies are similar to whole-cell studies subject to the caveat that patch formation may alter channel properties, and if channels are clustered, the patch may not be a representative sample of the cell. While the area-sampling problem is worse with single channel recordings, the extreme increase of resolution relative to multichannel recordings can reveal details such as multiple conducting states (Premkumar and Auerbach, 1997) that would otherwise be lost. Single channel analysis can also reveal heterogeneity that is averaged away with many-channel data (Premkumar and Auerbach, 1997).

Kinetic analysis tools utilizing maximum likelihood techniques permit a detailed analysis of nonstationary single or multiple channel activity to be completed within minutes (Feng et al., 1996; cf. www.qub.buffalo.edu). However, for these software tools to work well it is important that the molecular rate constants are independent of time, and for this to be true, the stimulus has to appear as a step.

Many methods have been developed to rapidly change concentration on a patch. These include photoactivation (uncaging; Niu et al., 1996a), U-tube perfusion, hydraulic switching between different flows (Maconochie and Knight,

Received for publication 21 January 1999 and in final form 27 April 1999.
Address reprint requests to Dr. Frederick Sachs, 124 Sherman Hall, SUNY, Buffalo, NY 14214. Tel.: 716-829-3289 ext. 105; Fax: 716-829-2028; E-mail: sachs@buffalo.edu.

0006-3495/99/08/682/09 $2.00

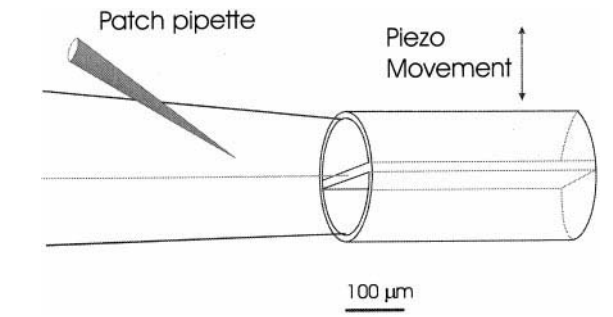

FIGURE 1 A diagram of a dual-stream system switcher made from theta tubing perfusing an outside-out patch.

1989), and physical translation of a pair of closely spaced streams across the patch (Jonas, 1995). The latter appears to be the most rapid of the hydraulic techniques. Compared to photoactivation (Niu et al., 1996a, b), solution switching doesn't require the synthesis of special compounds, and the rise time is often comparable. In optimal cases, however, photoactive release can work in the microsecond range (Niu et al., 1996b). Photorelease has the general limitations that it is not possible to make rapid transitions from high to low concentrations, and the actual concentrations are hard to determine.

The basic mechanism of a piezo solution switcher is shown in Fig. 1. Two streams of fluid leave a dual channel glass pipette in laminar flow with two different ligand concentrations (usually a zero and a test concentration). The channel diameters in the "theta" capillary are typically ~100 μm. To switch solutions, the pipette is rapidly translated normal to its axis, sweeping the flows across an excised patch at the end of a pipette.

The key factors controlling exchange time are the flow velocity, proximity of the patch to the exit port of the perfusion tube(s), translation velocity of the interface, steepness of the gradient, and exchange time of the unstirred layer. Only some of these factors can be estimated analytically. This paper deals with a quantitative evaluation of these factors.

METHODS

I did simulations made with a friendly finite element program, PDEase2 (Macsyma, Inc., Arlington, MA) running on a 400 MHz PC with 128 MB of memory. Convergence generally required only a few minutes. For simplicity and speed in the calculation, I exploited the symmetry of the problems, simulating only one of the flow streams. There were two kinds of simulation: steady-state calculations of concentration gradients in the flow and time-dependent calculations of the speed of exchange at the membrane. The geometric models were a compromise between the speed of calculation and useful analogy to the experimental conditions. For simulation of the washout speed, the standard geometry was a cylindrical patch pipette with radius of 1 μm concentric with a flow stream with a radius of 5 μm (shown to scale in Fig. 6). I tested different dimensions to evaluate the model sensitivity, but for moderate changes the differences were minor. For large bath spaces and for high velocities the program often didn't converge. Turbulence is not an issue, however, since the Reynolds number was always <1 and turbulence isn't expected until it exceeds 10^3. (The Reynolds number is a dimensionless scale factor for the similarity of flow. Re $= \rho v d/\eta$ where ρ is the density, v is the velocity, d is a characteristic dimension, and η is the viscosity (Granger, 1995)).

The calculation was carried out in two steps: 1) generating the flow field and 2) calculating the convection/diffusion process in the previously calculated flow field. This two-step approach greatly improved speed and

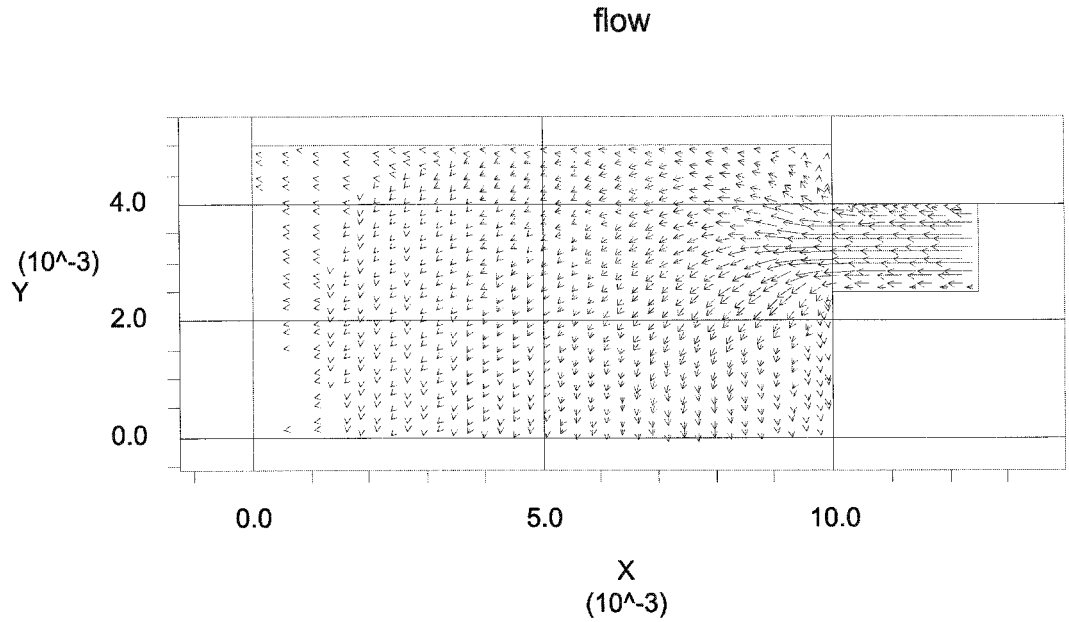

FIGURE 2 The flow field of a solution switcher. (Because of symmetry, only the bottom half is shown. Reflecting this half about the topmost line makes the full switcher). The entry port is at the right and the flow expands upward around the partition (20 μm wide for this simulation), to the left and downward into the bath. In this simulation the peak axial flow velocity is ~0.1 mm/s. The left and bottom sides represent the bath and the upper boundary the midline of the two streams. Axes are in centimeters.

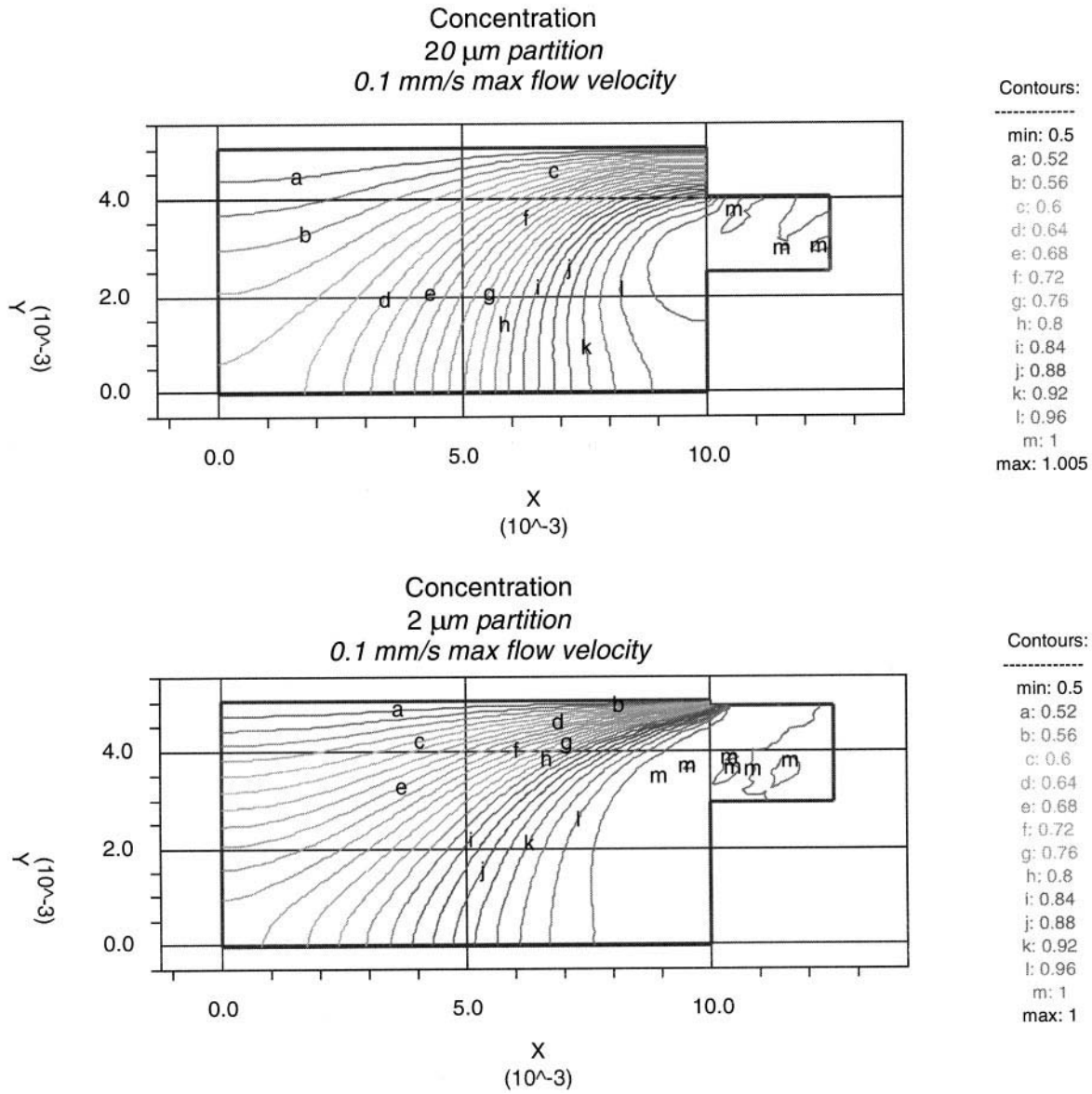

FIGURE 3 Concentration profiles for a switcher with two different partition widths (only the bottom half is shown because of symmetry). The flow, with unity concentration, enters at the right (*m* contours), the partition is above the influx channel and the top of the figure is the midline between the two streams. The left and bottom boundaries represent the bath solution. For the same flow rates, the concentration gradient at the end of the partition is much steeper for the narrow partition than for the wide partition. The flow rate on-axis in the inflow channel was ≈0.1 mm/s; the dimensions are in centimeters.

stability of the algorithms relative to a simultaneous solution. For small molecules that do not affect viscosity, diffusion does not influence flow and a single flow field will do for all variations in the concentration profile. The steady-state flow field was solved using the Navier-Stokes equations in Cartesian or cylindrical coordinates, as appropriate (Backstrom, 1994):

$$\rho(\vec{v}\cdot\nabla)\cdot\vec{v} + \nabla p - \eta\nabla^2\vec{v} = 0$$

where ρ is the fluid density, $\vec{v}$ the velocity vector (with z and r components), p is the pressure, and η is the viscosity. Because the Reynolds number was low, the density was set to 0 to increase the speed of calculations. Tests with $\rho = 1$ showed that this constraint made no detectable difference. The boundary conditions were set to uniform pressure at the input and zero at the output, zero velocity at all solid interfaces, and gradients unchanged at open boundaries. The velocity used to characterize the exchange time was the maximum entry velocity that was controlled by the input pressure. Because the flow stream did not change pattern with pressure in this low Reynolds number regime, for a fixed geometry I could simply scale the velocity field to different values to represent different input velocities. The viscosity was set to 1 cp for water.

The convection/diffusion equation for concentration C was solved using the flow field $\vec{v}$ just calculated (Carslaw and Jaeger, 1959):

$$\vec{v}\cdot\nabla C - D\nabla^2 C = -\partial C/\partial t$$

The diffusion constant $D = 10^{-5}$ cm^2/s unless otherwise stated. For steady-state calculations the concentration was set to 1 at the entry port, 0.5 at the midline between the streams, and the flux continuous at open boundaries. For time-dependent problems that simulated a step concentration in the flow stream, the initial conditions were $C = 1$ at the entry port, which became $C = 0$ at a distance ϵ from the patch. This unstirred layer thickness ϵ was nominally taken to be 1 μm, but I tested it at different values. This dimension is obviously arbitrary and was chosen as a measure of how close one might be able to approach the exit port of a solution

switcher. At a given flow velocity, increasing ϵ makes more time available for the step interface to relax to a sigmoid, thereby increasing the rise time (Crank, 1975). However, in the range explored ($\epsilon < 5$ μm), the main effect of increasing ϵ was to linearly increase the latency of the transition proportional to the flow velocity. Large increases in ϵ and low flow velocities significantly increase the rise time. In the following, rise time specifically means the time from 10% to 90% of the full response.

RESULTS

Analytic limits

The steepest possible gradient can be modeled as the apposition of two semi-infinite planes of different concentration, with time 0 representing when the two streams come into contact after leaving the ports. The solution for this diffusion problem between unit and zero concentrations is

$$C(x, t) = 0.5 * \text{erfc}(x/2\sqrt{Dt}) \quad (1)$$

where x is the distance from the boundary (the distance normal to the stream axis), D is the diffusion coefficient, and t is time (Carslaw and Jaeger, 1959). If we assume the closest the sample can be to the exit port is the patch radius, $r = 1$ μm. At 1 μm from the exit port with the maximum practical stream velocity $v = 100$ cm/s, the streams will have been in contact for $t = v/r = 1$ μs. For $D = 10^{-5}$ cm^2/s, 10–90% of the gradient will be covered within a distance of 0.1 μm. Laterally translating the streams (or the patch) at the same speed as the flow rate, 100 cm/s (1000 μm/ms), the gradient would be covered in $\sim$1 μs. This is the very best we can expect to do for small molecules in water.

Reducing the diffusion constant will increase the steepness of the gradient and reduce the demands for high translational velocities. If it is experimentally acceptable to raise the local viscosity of the perfusion solution, a 10-fold increase in viscosity (at the same velocity) will make the gradient $\sqrt{10}$ $\sim$3-fold steeper and reduce the exchange time by the same factor. The same reasoning suggests that when possible, agonists with the slowest diffusion rate should be used. As shown below, smaller diffusion constants also improve the washout time at the patch.

Effects of partition width

In the analytic calculations we assumed a zero thickness interface between the flow streams, but that is not possible in practice. The two streams join after leaving a separating partition of finite dimensions. The steepness of the gradient is affected by the width of this partition. The effect of the partition thickness cannot be easily calculated analytically, but is accessible to finite element modeling as discussed in Methods. Because PDEase could only simulate two spatial dimensions, I made a model of the perfusion pipette as two slots rather than two pipes. This model will give an upper estimate of the gradient because the diffusion and drag of the perfusate against the bath solution above and below the stream were ignored. By using the reflection symmetry of the two channels I simulated half of the switcher, and a typical flow pattern is shown in Fig. 2.

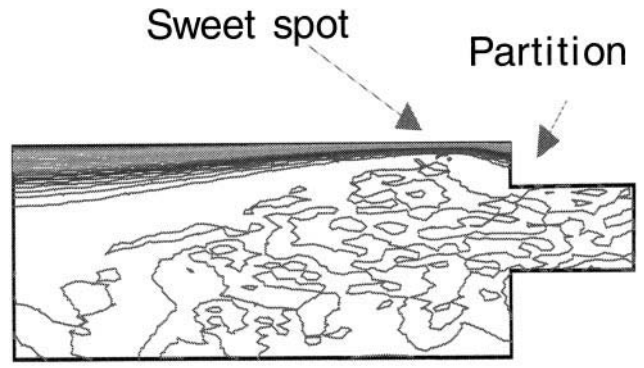

FIGURE 4 Concentration profiles for a 20-μm-wide partition showing the presence of the "sweet spot" $\sim$10 μm from the end of the partition. Maximum velocity is 5 cm/s from the right to left and the dimensions, except for the width of the partition, are as per Figs. 2 and 3.

The effect of different partition widths on the concentration gradient is shown in Fig. 3. The speed of perfusion clearly affects the gradient variation with distance.

The gradient of the transition region is narrower with the narrower partition. The width of the gradient is a monotonic function distance with a 1 μm partition, but a wider partition (Fig. 4) exhibits a "sweet spot"; a region of maximal gradient some distance from the exit port. The degree of narrowing and the placement of the spot is a function of flow velocity. Jonas noted the presence of this narrow region (Jonas, 1995).

For the 1 μm partition, the width of the gradient increases approximately as the square root of the velocity, as expected from the time allowed for diffusion in the infinite slab solution (Eq. 1). The 10 μm partition has shallower gradients because close to the exit port the stagnation layer allows relaxation of the gradient (cf. Tables 1 and 2). The extra diffusion time in the stagnation layer spreads the gradient so that it becomes insensitive to the distance from the port (*lower traces* in Fig. 5, *top*) until the distance is $>$50 μm. Again, because of the stagnation layer, the gradient very close to the port (1 μm in Fig. 5, *top*) is wider than further away: the "sweet spot" syndrome.

TABLE 1 Summary: the effect of flow velocity on the width (10–90%) of the concentration gradient as a function of distance from the exit port (1 μm partition)

Distance from exit port (μm)	Regression of 10–90% width (μm) of gradient versus flow velocity (cm/s)
1	$w_{10-90} = 2.3v^{-0.40}$
5	$w_{10-90} = 3.4v^{-0.48}$
10	$w_{10-90} = 4.5v^{-0.42}$
20	$w_{10-90} = 7.3v^{-0.53}$
50	$w_{10-90} = 25.2v^{-0.53}$

TABLE 2 Summary: the effect of flow velocity on the width (10–90%) of the concentration gradient as a function of distance from the exit port (10 μm partition)

Distance from exit port (μm)	Regression of 10–90% width (μm) of gradient versus flow velocity (cm/s)
1	$w_{10-90} = 6.0v^{-0.35}$
5	$w_{10-90} = 5.4v^{-0.45}$
10	$w_{10-90} = 5.2v^{-0.46}$
20	$w_{10-90} = 6.7v^{-0.49}$
50	$w_{10-90} = 18.7v^{-0.43}$

The unstirred layer

A practical upper limit on the speed of exchange is how fast the patch can be wiped free of the previous concentration by the incoming fluid. The region around the patch is subjected to both convection and diffusion, and the role of the geometry is not easy to assess analytically. A full analysis would require a four-dimensional simulation that would track movement of the solution interface in three dimensions as function of time. This moving boundary problem is notoriously difficult to solve. As a significant simplification I used a cylindrically symmetric geometry with a step concentration jump created in the flow stream. The location of this jump could be set at different distances from the patch corresponding roughly to the distance from the patch to the exit port (Fig. 6). The velocity flow field under the standard conditions is shown in Fig. 7 with contours of velocity in the axial z direction.

There is no circulation as expected from the geometry and low Reynolds number. The shape of the flow field is independent of velocity and the velocity is linearly proportional to the pressure drop. If the pipette is removed from the simulation domain, the flow field is accurately parabolic, as expected for a cylindrical tube (Backstrom, 1994).

With a step gradient of concentration imposed on the flow field, the concentration at the patch is sigmoidal in time. Fig. 8 shows an example at a flow velocity of 1 cm/s. At this velocity and dimensions, the concentration at the center of the patch and the edge of the patch are nearly identical over time with a rise time of ~370 μs.

At both higher and lower flow velocities there is increased dispersion, with the edge exchanging faster than the center. The dispersion can be comparable to the rise time as shown in Fig. 9 and might be significant for detailed quantitation. What is remarkable at high flow speeds is the rapidity of exchange. At 100 cm/s it would appear that the exchange could be accomplished within 3 μs if a step

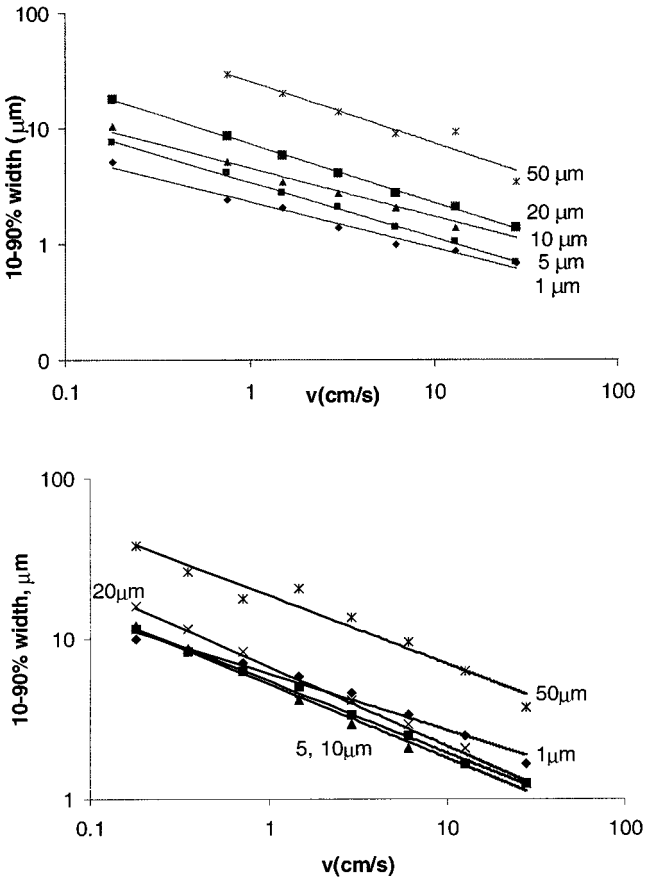

FIGURE 5 The effect of flow velocity on the width (10–90%) of the concentration gradient as a function of distance from the exit port for a 1-μm partition (*top*) and 10-μm partition (*bottom*). The distances on the plot are the distances from the exit port. The solid lines are regressions to a power law (see Table 1). Notice the top plot has three log units on its ordinate and the lower has two.

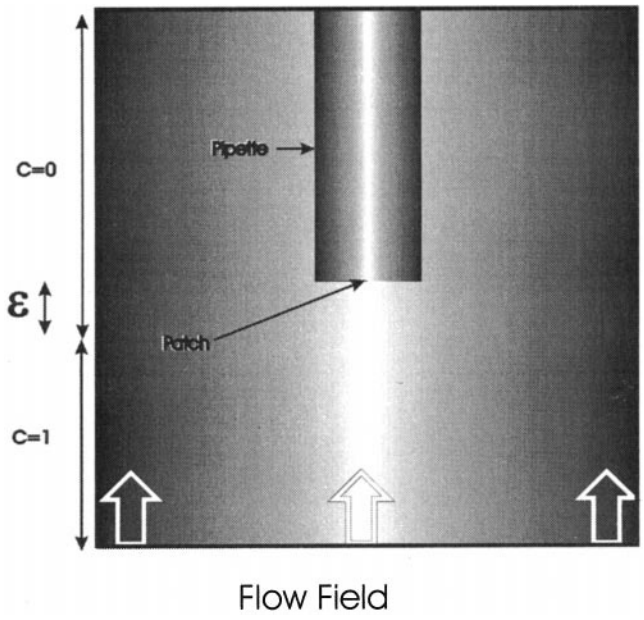

FIGURE 6 Diagram of the simulation geometry. The flow field is parabolic in z at the entry port. The initial conditions for calculating the time-dependence of the concentration (C) is shown at the left. The simulation starts with a unit step of C at a distance ϵ from the patch. The actual numerical simulation involved only the left half of the drawing utilizing the radial symmetry of the problem.

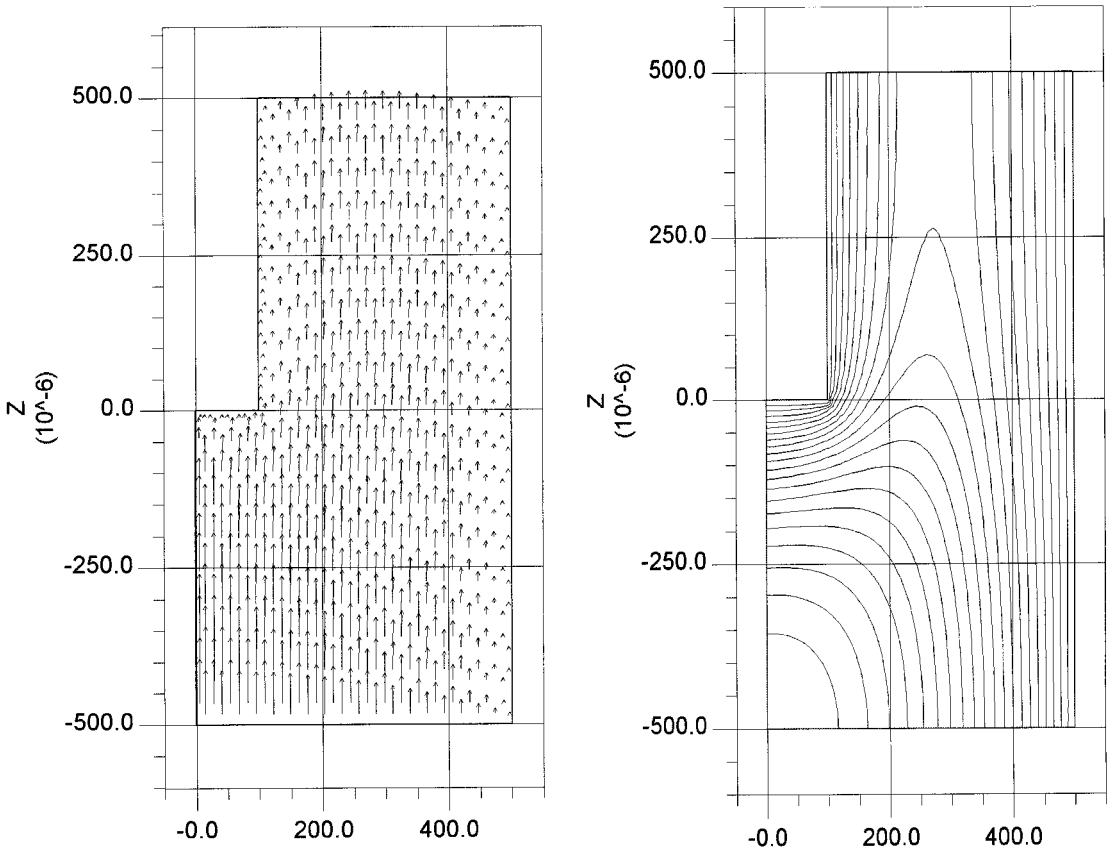

FIGURE 7 (*Left*) Flow field with the flow moving from bottom to top. (*Right*) The contours of constant z velocity 0.05 cm/s apart; the maximum velocity is 1 cm/s (inflow axis is at the lower left of the diagram). The geometric units are centimeters $\times 10^6$, i.e., 400 means 4 μm. The computation made use of cylindrical symmetry so the simulated domain was only half of the full geometry.

gradient can be created. At low flow velocities, the concentration time course becomes dominated by a slow tail characteristic of the error function time course of diffusion across an initial step (Carslaw and Jaeger, 1959; Fig. 10).

The relationship of rise time (RT) to flow velocity can be well-described by a power law relationship (Fig. 11). For the standard geometry, where v is the maximal z component of velocity, $RT = 572 * v^{-1.35}$.

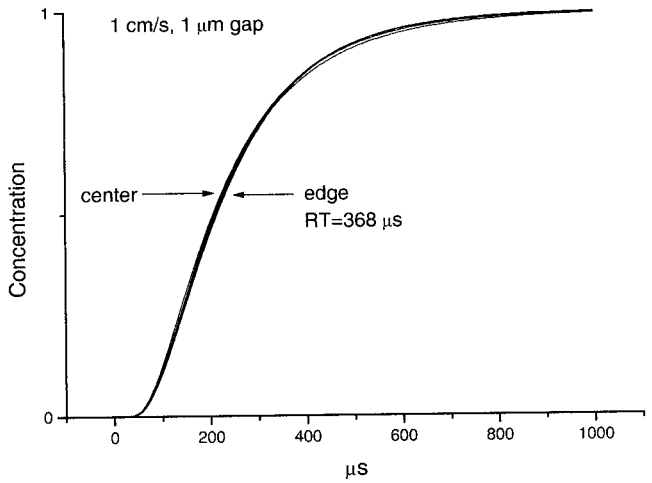

FIGURE 8 The concentration at the patch versus time at $v = 1$ cm/s and the standard geometry: patch radius = 1 μm, $\epsilon = 1$ μm, port radius = 5 μm. The concentration at the center and the edge of the patch have nearly equal response times at this flow rate and geometry. The 10–90% rise time is 360 μs.

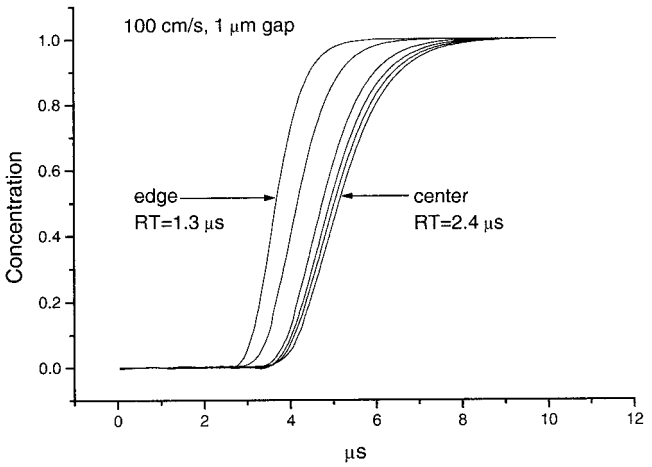

FIGURE 9 The concentration versus time at $v = 100$ cm/s and the standard geometry (see Fig. 7). The 10–90% rise time is 1.3 μs at the edge of the patch and 2.4 μs at the center. The dispersion of rise times is comparable to the magnitude of the rise times. The curves are sampled at 0, 0.2, 0.33, 0.5, 0.75, and 0.9 μm from the center of the patch.

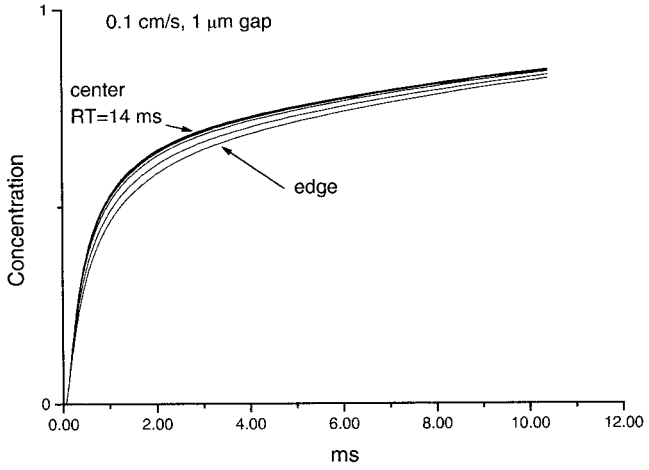

FIGURE 10 The concentration versus time at $v = 0.1$ cm/s and the standard geometry (see Fig. 7). The 10–90% rise time is quite slow, being 14 ms at the center of the patch.

Variation of the simulation parameters generally produced reasonable results. If the dead space ϵ was increased from the standard 1 μm to 5 μm, the rise times were nearly unaffected, but the latency increased from ~5 to 9 μs. At 100 cm/s this increase of 4 μm is covered in 4 μs, while the extent of diffusion in that time is small.

Decreasing the diffusion constant (to represent perfusion with larger molecules) has the effect of maintaining a steep gradient, thereby decreasing the rise time. The rise times for molecules with different diffusion constants are shown in Table 3. Decreasing the diffusion constant emphasizes the convective versus the diffusive components of the concentration relaxation. The saturation in rise time with decreasing diffusion constant represents domination by convection.

The decrease in rise time with the decrease in diffusion constant (at constant flow rate) suggests a possible tool for speeding up solution exchange. However, a factor of two seems a practical maximum under these conditions. The rise time is not strongly dependent on the diameter of the patch. The recursion of rise time against flow velocity for different diameter patches is shown in Table 4. Smaller patches exchange faster, but the effect is only significant (3-fold) at 100 cm/s.

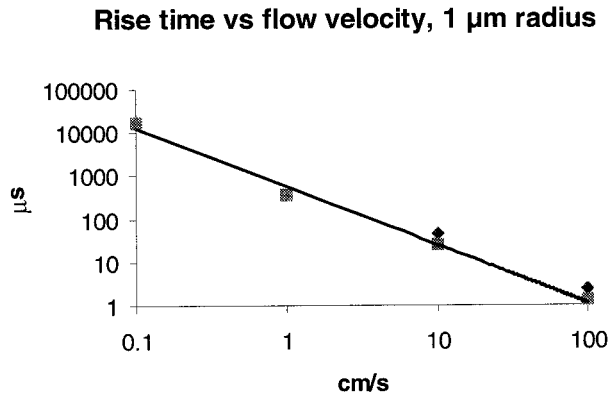

FIGURE 11 The rise time as a function of maximal flow velocity for the standard geometry. The diamonds and squares, respectively, represent the rise time at the center and the edge of the patch. The regression is essentially the same for both. The slight positive deviation at low velocities appears to be an effect of the finite width of the simulated domain.

TABLE 3 The effect of diffusion constant on the rise time of concentration on a patch

Diffusion constant (cm^2/s)	RT_c (μs)	RT_e (μs)
10^{-5}	45	26
10^{-6}	23	13
10^{-7}	22	12

Standard geometry, $v = 10$ cm/s, RT_c and RT_e, respectively center and edge of patch.

DISCUSSION

This study suggests that if perfusion velocities are kept rapid, in principle we can exchange solutions in microseconds. The unstirred layer around the patch is not rate-limiting; the issue is how to move from one solution to the next in microseconds. For a given translational velocity of the ports, the sharper the interface between the solutions, the more rapid the solution exchange. The prime variable is the flow velocity; the faster the flow, the faster the exchange. The maximum flow velocity is determined by stability of the patch and Jonas (1995) claims 10–15 cm/s (μm/ms) is usable. At 10 cm/s, the dynamic pressure, $\rho v^2/2$ (Granger, 1995), is 50 dyne/cm^2 (0.5 cm water). This is a minor pressure relative to that used to stimulate mechanosensitive channels in patches (Hamill and McBride, Jr., 1995). Patch failure under flow may instead be caused by collision with contaminating particles (Jonas, 1995). Although the traditional placement of the patch pipette is pointing upstream, placement normal to the flow direction will reduce both the transmembrane pressure gradient and the particle collision frequency. Simulations indicate that the washout times are not very different in the two orientations: there is no stagnation layer when the pipette axis is normal to the flow.

There are four other factors that influence the steepness of the gradient. The first is proximity to the exit ports. Because the diffusion between the two streams begins the moment they meet, the closer the patch is to the exit port, the faster the rise time. The second factor is the width of the partition between the two ports. The narrower the partition,

TABLE 4 The variation of rise time (10–90%) with velocity for different sized patches

Patch radius, μm	Regression: mean RT_{10-90} (μs) vs. v (cm/s)
0.5	$RT = 458v^{-1.42}$
1.0	$RT = 572v^{-1.35}$
2.0	$RT = 869v^{-1.27}$

For all regressions $R^2 > 0.98$.

the less time the two solutions spend in contact with the dead space at the end of the partition. The third factor is the viscosity of the solutions. The higher the viscosity, the lower the diffusion constant and the more slowly the diffusion gradient relaxes. Finally, there is the translational velocity of the ports. The faster the ports move, the more rapidly they cross the indeterminate concentrations between the two streams.

The width of the partition between the streams is important (cf. Fig. 4). The wider the partition, the lower the gradient at all distances. The theta glass for perfusion pipettes should have narrow partitions. Alternatively, silicon microlithography allows a precise control of port and partition geometry (Beyder and Sachs, 1998). With a narrow partition, the key to maintaining a sharp gradient is proximity to the exit port. Narrowness of the gradient is important because it permits the use of short-travel, high-speed piezo translators.

Although it appears not to have been used as a tool in rapid switching experiments, increasing the viscosity appears to help to maintain the gradient. It should be pointed out that relevant viscosity must be the local viscosity, and not a long-range effect, such as caused by the addition of polymers. Unfortunately, increasing the viscosity may not be an insignificant perturbation of channels in the patch and will certainly decrease channel currents. The usefulness of increased viscosity will depend upon the specifics of the channels under study.

Once the steady-state gradient is established, the rate-limiting step is how fast the patch crosses the gradient. Typical piezoelectric motors may translate 50 μm in 1 ms (Jonas, 1995). This is a velocity of 5 cm/s, slower than the maximal fluid stream velocities. A reasonable choice of speed is to translate the exit ports so that the time to cross the gradient is the same as the exchange time in the unstirred layer. Combining the regressions from Tables 1 and 4 with a little manipulation, we can get a simple formula that, to first-order, predicts the optimal velocity v_T (cm/s) as a function of the distance d (μm) from the port and the flow velocity v (cm/s):

$$v_T = 0.45 * e^{0.05d} v \quad (2)$$

The frequency response f of the piezo can be estimated from the rise time (assuming a first-order response):

$$f(\text{kHz}) = 0.28 v^{1.35} \quad (3)$$

A plot of Eq. 2 is shown below in Fig. 12. The closer the patch is placed to the port, the smaller the required translation velocity and the less the demand on the piezo motor. Lower velocities make it easier to find piezo motors that will satisfy the optimal frequency response requirements (Fig. 13). While one need not work precisely at the "optimal" settings, there is little to be gained from much faster perfusion rates if the patch can't be translated rapidly across the gradient. It would appear from Fig. 13 that perfusion rates of 10–15 cm/s are the practical maxima and have been shown to be usable in the laboratory. These rates require piezo responses of 5–10 kHz. Referring to Fig. 11, at ~10 cm/s the rise time cannot be <20 μs because of the limited rate of washout from the unstirred layer. At higher flow rates, the rate-limiting step becomes translation of the interface across the patch. It appears that with proper design of the switcher, it is reasonable to expect that the concentration on a patch can be changed in 20 μs.

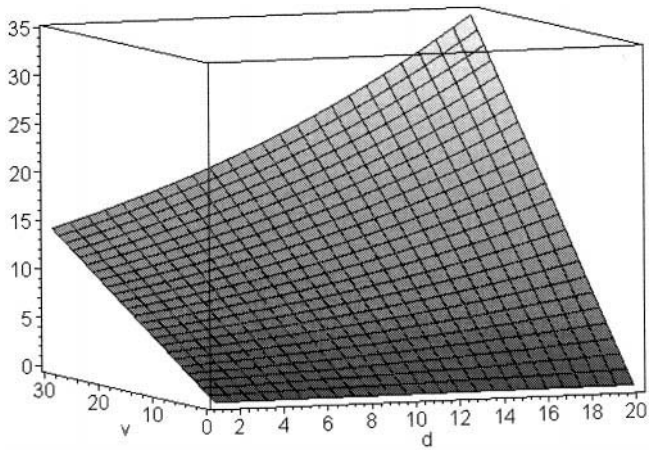

FIGURE 12 A plot of the optimal translation velocity (cm/s) versus the flow velocity v (cm/s) and the distance d (μm) from the exit port (1 μm radius patch).

The same dual stream technology can be applied to temperature jump experiments using streams at different temperatures. The main difference is that heat diffuses ~14 times faster than small molecules. This means that the thermal gradients will relax faster, so that at 10 cm/s the rise time for a thermal gradient will be ~65 μs (for comparison to mass diffusion see Table 3). In practice, it will be somewhat slower because the thermal capacity and conductivity of the water-filled patch pipette is not included in the simulation. It is reasonable to expect 100 μs positive and negative temperature jumps using a switcher. Although this is slow compared to a heating pulse from a laser, the laser can only raise the temperature, whereas the switcher is bipolar.

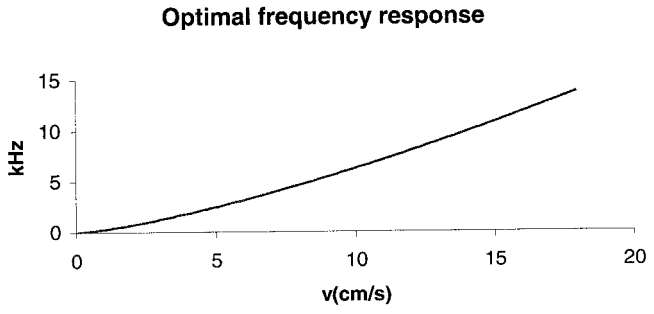

FIGURE 13 The frequency response of the piezo translator needed to move a patch across the gradient at the optimal speed as a function of the flow velocity (1 μm radius patch).

I thank Arthur Beyder for assistance in the early simulations and for building photolithographic silicon mixing ports that may prove capable of implementing some of the ideas presented here.

This work was supported by grants from the National Institutes of Health, United States Army Research Office, and a Small Business Innovation Research Grant in collaboration with Burleigh Instruments.

REFERENCES

Backstrom, G. 1994. Fields of Physics on the PC by Finite Element Analysis. Studentlitteratur, Lund, Sweden.

Benndorf, K. 1995. Low-noise recording. *In* Single Channel Recording. B. Sakmann and E. Neher, editors. Plenum, New York. 129–146.

Beyder, A., and F. Sachs. 1998. Cornell Nanofabrication Facility Annual Report 1997–1998. Cornell University, Ithaca, NY. 26–27.

Carslaw, H. S., and J. C. Jaeger. 1959. Conduction of Heat in Solids. Clarendon, Oxford.

Colquhoun, D., P. Jonas, and B. Sakmann. 1992. Action of brief pulses of glutamate on AMPA/kainate receptors in patches from different neurones of rat hippocampal slices. *J. Physiol. (Lond.)*. 458:261–287.

Crank, J. 1975. The Mathematics of Diffusion. Clarendon, Oxford.

Feng, Q., A. Auerbach, and F. Sachs. 1996. Estimating single channel kinetic parameters from idealized patch-clamp data containing missed events. *Biophys. J.* 70:264–280.

Granger, R. A. 1995. Fluid Mechanics. Dover Publications, Mineola, NY.

Hamill, O. P., and D. W. McBride, Jr. 1995. Pressure/patch-clamp methods. *In* Neuromethods. A. Boulton, G. Baker, and W. Walz, editors. Humana Press Inc., Totowa, NJ. 75–87.

Horn, R., and C. A. Vandenberg. 1984. Statistical properties of single sodium channels. *J. Gen. Physiol.* 84:505–534.

Jonas, P. 1995. Fast application of agonists to isolated membrane patches. *In* Single-Channel Recording. B. Sakmann and E. Neher, editors. Plenum Press, New York. 231–243.

Kienker, P. 1989. Equivalence of aggregated Markov models of ion-channel gating. *Proc. R. Soc. Lond. Biol. Sci.* 236:269–309.

Maconochie, D. J., and D. E. Knight. 1989. A method for making solution changes in the sub-millisecond range at the tip of a patch pipette. *Pflugers Arch.* 414:589–596.

Maconochie, D. J., J. M. Zempel, and J. H. Steinbach. 1994. How quickly can GABAA receptors open? *Neuron.* 12:61–71.

Niu, L., R. W. Vazquez, G. Nagel, T. Friedrich, E. Bamberg, R. E. Oswald, and G. P. Hess. 1996a. Rapid chemical kinetic techniques for investigations of neurotransmitter receptors expressed in Xenopus oocytes. *Proc. Natl. Acad. Sci. USA*. 93:12964–12968.

Niu, L., R. Wieboldt, D. Ramesh, B. K. Carpenter, and G. P. Hess. 1996b. Synthesis and characterization of a caged receptor ligand suitable for chemical kinetic investigations of the glycine receptor in the 3-microseconds time domain. *Biochemistry*. 35:8136–8142.

Premkumar, L. S., and A. Auerbach. 1997. Stoichiometry of recombinant N-methyl-D-aspartate receptor channels inferred from single-channel current patterns. *J. Gen. Physiol.* 110:485–502.

Ruknudin, A., M. J. Song, and F. Sachs. 1991. The ultrastructure of patch-clamped membranes: a study using high voltage electron microscopy. *J. Cell Biol.* 112:125–134.

Sakmann, B., and E. Neher. 1984. Patch clamp techniques for studying ionic channels in excitable membranes. *Annu. Rev. Physiol.* 46: 455–472.

Sokabe, M., F. Sachs, and Z. Jing. 1991. Quantitative video microscopy of patch clamped membranes: stress, strain, capacitance, and stretch channel activation. *Biophys. J.* 59:722–728.